Photoluminescence from $In_{0.5}Ga_{0.5}As$/GaP quantum dots coupled to photonic crystal cavities

Kelley Rivoire,[1,*] Sonia Buckley,[1] Yuncheng Song,[2] Minjoo Larry Lee,[2] and Jelena Vučković[1]
[1]*E. L. Ginzton Laboratory, Stanford University, Stanford, California 94305, USA*
[2]*Department of Electrical Engineering, Yale University, New Haven, Connecticut 06511, USA*
(Received 3 November 2011; revised manuscript received 2 January 2012; published 23 January 2012)

We demonstrate room-temperature visible-wavelength photoluminescence from $In_{0.5}Ga_{0.5}As$ quantum dots embedded in a GaP membrane. Time-resolved above band photoluminescence measurements of quantum dot emission show a biexpontential decay with lifetimes of ≈200 ps. We fabricate photonic crystal cavities which provide enhanced outcoupling of quantum dot emission, allowing the observation of narrow lines indicative of single quantum dot emission. This materials system is compatible with monolithic integration on Si and is promising for high-efficiency detection of single quantum dot emission as well as optoelectronic devices emitting at visible wavelengths.

DOI: 10.1103/PhysRevB.85.045319 PACS number(s): 78.67.Hc, 42.72.Bj, 68.65.Hb

I. INTRODUCTION

Quantum dot emitters grown in gallium phosphide are important for both classical optoelectronic and quantum applications. The close match between the lattice constants of GaP and Si [0.37% at 300 K (Ref. 1)] is promising for monolithic integration with silicon,[1–3] and the large electronic band gap of GaP allows light emission at visible wavelengths. Single quantum dots (QDs) at visible wavelengths are beneficial for quantum applications since Si avalanche photodiodes (APDs) have maximum quantum efficiencies in the red part of the spectrum; additionally, emission in this part of the spectrum can be frequency downconverted to telecommunications wavelengths using readily available lasers.[4,5]

Quantum dots emitting in the red have been extensively studied over the past decade in materials systems, including InP/InGaP,[6–9] InP/GaP,[10,11] InP/AlGaInP,[12,13] GaInP/GaP,[14] InAs/GaP,[15] and AlGaInP/GaP.[16] Of these systems, clear single quantum dots with narrow emission lines exhibiting antibunching have been observed only in the InP/InGaP and InP/AlGaInP systems. GaP-based materials, by contrast, allow either monolithic integration with Si or growth on a nonabsorbing GaP substrate (due to the large indirect electronic band gap); additionally, the stronger second-order optical nonlinearity of GaP compared to InGaP is preferable for on-chip frequency downconversion to telecom wavelengths. Recently,[17] low-temperature emission (80 K) was measured from $In_{0.5}Ga_{0.5}As$ self-assembled QDs in GaP emitting in the red part of the spectrum. This system provides large wavelength tunability as the In fraction can be varied from 0.07–0.50 without introducing dislocations; additionally, it should provide deeper confinement for carriers than InP/GaP. Subsequently, room-temperature emission was measured from $In_{0.3}Ga_{0.7}As$/GaP QDs;[18] the measured temperature dependence of emission and supporting tight-binding calculations indicated good confinement of the carriers and type-I emission. Here, we further characterize this materials system, integrate it with photonic nanostructures that enhance the emission of the QDs, and observe evidence indicative of emission from individual QDs.

II. TEMPERATURE DEPENDENT PHOTOLUMINESCENCE

The QDs are grown by solid-source molecular-beam epitaxy (MBE) in the center of a 200-nm-thick GaP membrane grown on top of a 500-nm layer of $Al_{0.8}Ga_{0.2}P$ on a (001) GaP substrate. Figure 1(a) shows the measured QD photoluminescence (PL) as a function of temperature from 25 K to 300 K in a continuous-flow helium cryostat using 700-μW excitation power from a 405-nm continuous-wave (CW) diode laser. (The power level was chosen to maintain a constant integration time on the spectrometer CCD for all temperatures.) The center wavelength of the QD emission redshifts by 30 nm from 25 K to 300 K. The large full width half maximum of the emission is expected to result from inhomogeneous broadening due to variation in the physical size of the QDs.[17] Figure 1(b) shows that for higher pump powers, the QD spectrum broadens on the high-energy side and the integrated intensity is nonlinear as a function of power, indicating the presence of excited states. To characterize the confinement of carriers in the QDs, we study the intensity of QD emission as a function of temperature. Figure 1(c) shows the emission intensity integrated across the low-energy half of the QD PL spectrum (to minimize the contribution of excited states) from Fig. 1(a). The emission intensity decreases by a factor of 4 from cryogenic temperatures to room temperature. Figure 1(d) shows a fit of this integrated intensity to an Arrenhius model (assuming a temperature-independent radiative lifetime) with a single activation energy with the form

$$\frac{I(T)}{I_0} = \frac{1}{1 + C\left(\exp\frac{-E_a}{kT}\right)}, \tag{1}$$

where $I(T)$ is the temperature-dependent intensity, I_0 is the intensity at 0 K, C is a constant, k is Boltzmann's constant, and E_a is the activation energy indicating carrier confinement. We measure $E_a = 161$ meV; this is slightly larger than the 134 meV measured by Tranh *et al.*,[18] most likely due to the larger indium content in our samples thus resulting in deeper confinement.

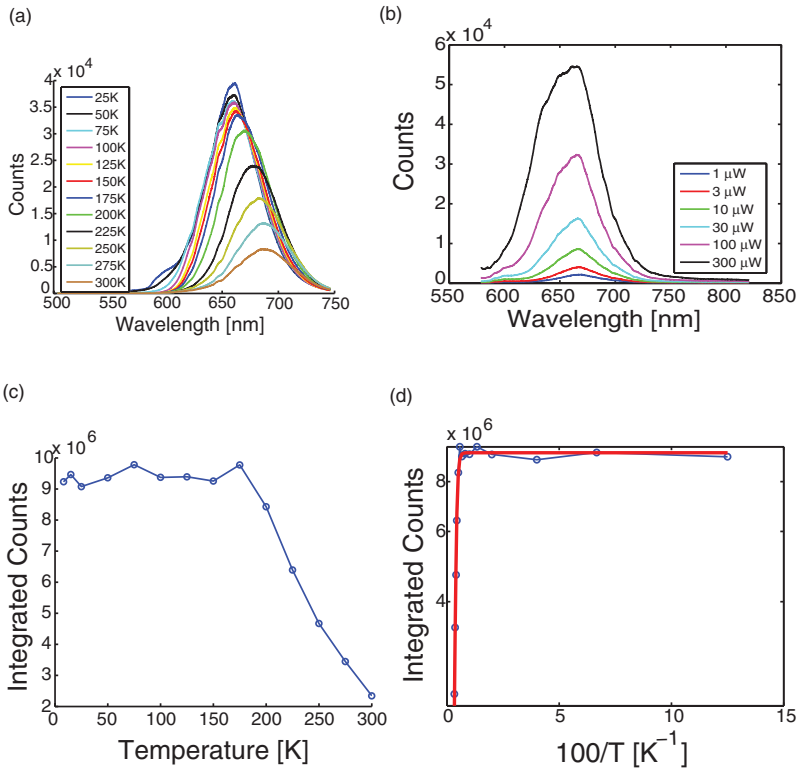

FIG. 1. (Color online) (a) QD PL from an unprocessed region of the sample as temperature is varied between 25 K and 300 K. The pump is a 405-nm CW laser diode at 700 μW. (b) Photoluminescence as a function of pump power at 10 K showing broadening at higher energies with increasing power, indicative of the presence of excited states. (c) Integrated counts of the low-energy half of the PL spectrum (to minimize the contribution of the excited states, which varies with temperature). Intensity is decreased by a factor of 4 at 300 K. (d) Semilog plot of integrated counts of the low-energy half of the PL spectrum versus inverse temperature. The fit to the exponential (solid red line) gives the activation energy $E_a = 161$ meV.

III. TIME-RESOLVED PHOTOLUMINESCENCE

We investigate the dynamics of the ensemble-QD emission by studying the time-resolved photoluminescence on a streak camera when the quantum dots are excited at 400 nm by a frequency-doubled Ti:Sapphire laser with a repetition rate of 80 MHz. The experimental setup is shown in Fig. 2(a); the instrument response to the pump (12 ps) is shown in the inset of Fig. 2(b). The time-resolved emission of the low-energy

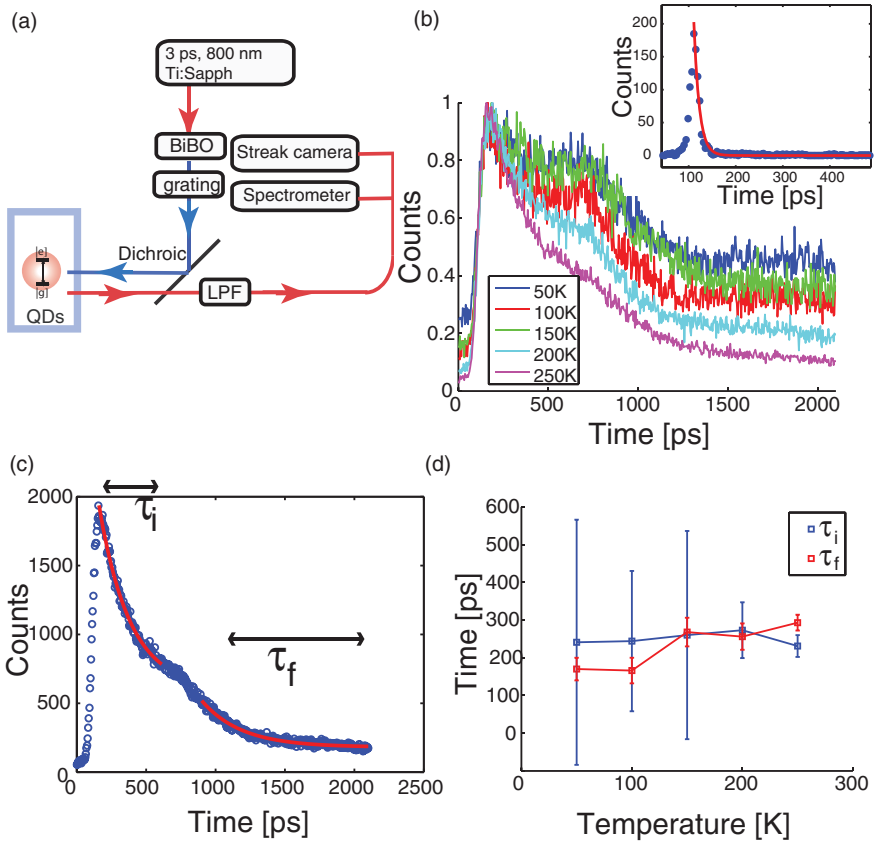

FIG. 2. (Color online) (a) Experimental setup for time-resolved measurements. 3-ps pulses at 800 nm from a Ti:Sapphire laser are frequency doubled in a BiBO crystal. A grating is used to filter the 400-nm light, which is passed through a dichroic mirror onto the sample. The photoluminescence emitted by the quantum dots is transmitted through the dichroic, passed through a long-pass filter (LPF) to remove any residual pump, and sent to a spectrometer or streak camera (for time-resolved measurements). (b) Time-resolved streak-camera measurements showing the lifetime integrated across the low-energy half of the PL spectrum for different temperatures. Inset: The excitation pulse at 400 nm. The red line indicates the fit with a decay time of 12 ps, limited by instrument resolution. (c) Exponential fits (red solid line) of time-resolved data at 250 K, showing initial and final decay times τ_i and τ_f. (d) Measured lifetimes as a function of sample temperature.

half of the QD spectrum [Fig. 2(b)] for all temperatures shows a biexponential decay with a short component ($\tau_i \approx 250$ ps, averaged across all temperatures), followed by a decay with a similar time constant ($\tau_f \approx 230$ ps) after a delay of ≈500 ps. The delay is most likely indicative of the phonon-assisted transfer of carriers from the indirect GaP matrix.[10] Figure 2(c) shows the time-resolved PL measured at 250 K, indicating regions used for fitting initial and final time constants. The extracted time constants for each temperature are shown in Fig. 2(d); error bars indicate error from the fit. The short lifetime is consistent with a type-I system; the minimal temperature dependence of decay rates indicates the absence of temperature-dependent nonradiative processes.

IV. ENHANCED OUTCOUPLING VIA PHOTONIC CRYSTAL CAVITY

To fabricate photonic crystal cavities, we used a different sample with a thinner 93-nm-thick GaP membrane for ease in fabrication. The photonic crystals were fabricated by top-down fabrication, including e-beam lithography, dry etching, and wet etching to remove the sacrificial AlGaP layer.[19] A scanning-electron-microscope (SEM) image of a fabricated sample is shown in Fig. 3(a) . Due to a difference in MBE growth parameters, the emission wavelength of the thinner sample was slightly blueshifted as shown in Fig. 3(b), and the QD density was lower. Figure 3(c) shows photoluminescence, measured at 12 K, from the quantum dots coupled into the linear three-hole-defect photonic crystal cavity.[20] The fundamental mode of the cavity with the highest quality factor (black circle) overlaps with the tail of the QD emission; the brighter higher-order cavity modes[21] are more closely matched to the QD-emission spectrum. Figure 3(d) shows the fundamental cavity-mode resonance at 681.7 nm; a Lorentzian fit indicates a quality factor of 2800, and Fig. 3(e) shows a finite-difference–time-domain (FDTD) simulation of the spatial distribution of the electric-field intensity in the center of the membrane for this cavity mode.

By measuring the cavity-enhanced QD emission, we are able to observe indications of single quantum dot emission lines at temperatures below 60 K. Figure 4(a) shows the low-temperature-PL spectrum with a CW pump from another photonic crystal cavity on the chip. The black circle indicates the higher-order mode of interest which we use to enhance the quantum dot emission outcoupling. The inset shows the spatial profile of the electric-field intensity for the mode of interest, calculated by the FDTD method. Figure 4(b) shows a high-resolution spectrum measured at 10 K of the QD and cavity mode at 610 nm [black circle in Fig. 4(a)]. At low power, two narrow lines appear to saturate (as would be expected for single QDs) as power is increased above about 30 μW. At higher powers, we recover the Lorentzian line shape of the photonic crystal cavity mode as the intensity in the cavity mode continues to grow while the intensity from the individual QD lines has saturated. Figure 4(c) shows the wavelength shift of the quantum dots and cavity as a function of temperature, indicating a quadratic redshift in dot emission as temperature is increased as expected due to the approximately quadratic shift in material band gaps in this temperature range.[22] Quantum dot lines are measured at 500 nW (far below QD saturation) while the cavity is measured at 100 μW (above QD saturation). The quantum dot emission wavelength changes at a different rate than the cavity emission, confirming that the narrow lines are not associated with a cavity

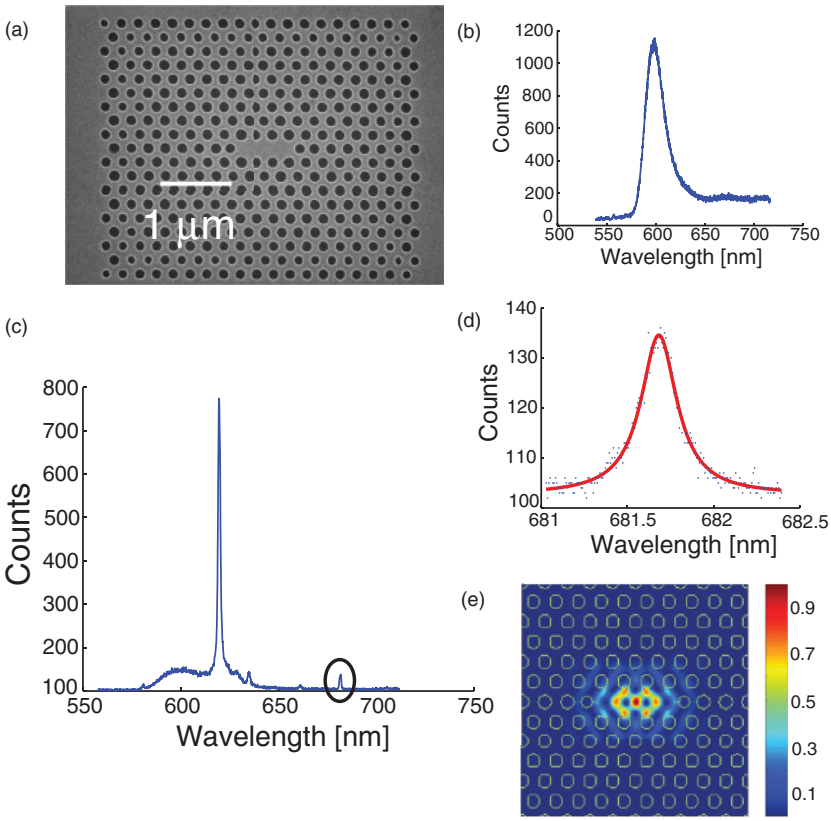

FIG. 3. (Color online) (a) SEM image of a photonic crystal nanocavity. (b) PL measured at 12 K with the 405-nm CW pump from an unprocessed region of thinner sample used for photonic-crystal measurements. The QD wavelength is slightly blueshifted from Fig. 1. (c) PL measurement indicating the emission of quantum dots coupled into cavity modes. The fundamental cavity mode is indicated by the black circle. (d) Lorentzian fit (red solid line) of the fundamental cavity mode at 681.7 nm with $Q = 2800$. (e) FDTD-simulated electric-field intensity for the fundamental cavity mode.

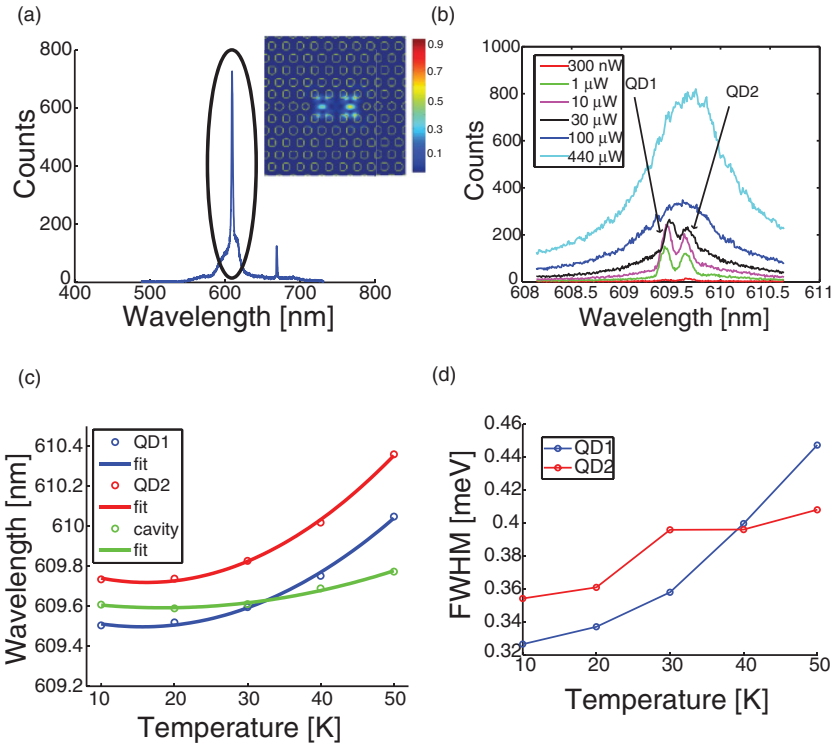

FIG. 4. (Color online) (a) PL from a different photonic-crystal-cavity structure with the higher-order cavity mode aligned to the wavelength of the strongest QD PL measured with the 405-nm CW pump. The black circle indicates the mode of interest. Inset: The FDTD-simulated electric-field intensity for the higher-order cavity mode indicated by the circle in (a). (b) High-resolution spectra of QD PL from the cavity in (a). Measurements are taken at 10 K. The two single lines at low power are indicative of single quantum dots. (c) The change in wavelength of quantum dots (measured at 500 nW) and cavity (measured at 100 μW) as a function of temperature. Solid lines indicate quadratic fits. (d) Change in QD linewidth as a function of temperature.

mode. Figure 4(d) shows the change in the full width at half maximum (FWHM) of the observed spectral lines at 1 μW power as a function of the temperature measured. The narrow QD-like lines show an increase in linewidth as the temperature is raised, as expected for single quantum dots, while the cavity linewidth remains roughly unchanged in the same temperature range. Further confirmation of single QD behavior could be obtained from photon-statistics measurements. We did not obtain a sufficient signal-to-noise ratio from the cavity to perform such measurements in this case. An improvement in the signal-to-noise ratio, for example by improving the cavity quality factor, would also allow an investigation of the time-resolved dynamics of a single QD coupled to the cavity where Purcell enhancement is expected in this regime.[23]

V. CONCLUSION

In conclusion, we measure the temperature-dependent photoluminescence from $In_{0.5}Ga_{0.5}As$ quantum dots embedded in a GaP membrane, indicating good carrier confinement with only a fourfold decrease in emitted intensity from cryogenic to room temperature. We study the temperature-dependent time-resolved photoluminescence, which shows a biexponential decay with time constants of ≈200 ps. We also observe enhanced emission into the modes of a photonic crystal cavity and narrow lines consistent with single-quantum-dot emission. The materials system is compatible with monolithic integration on Si and is also promising for quantum applications. The quantum dot wavelength is matched to the high-efficiency region of silicon APDs and could be downconverted to telecommunication wavelengths through integration with photonic nanostructures.[24–27]

ACKNOWLEDGMENTS

This work was supported by the National Science Foundation, a National Science Graduate Fellowship, and Stanford Graduate Fellowships. M.L.L. acknowledges the DARPA Young Faculty Award program (Grant No. N66001-11-1-4148).

*krivoire@stanford.edu

[1]T. J. Grassman, M. R. Brenner, S. Rajagopalan, R. Unocic, R. Dehoff, M. Mills, H. Fraser, and S. A. Ringel, Appl. Phys. Lett. **94**, 232106 (2009).
[2]A. C. Lin, J. S. Harris, and M. M. Fejer, J. Vac. Sci. Technol., B **29**, 03C120 (2011).
[3]N. Talebi and M. Shahabadi, J. Opt. Soc. Am. B **27**, 2273 (2010).
[4]N. Curtz, R. Thew, C. Simon, N. Gisin, and H. Zbinden, Opt. Express **18**, 22099 (2010).
[5]S. Zaske, A. Lenhard, and C. Becher, Opt. Express **19**, 12825 (2011).
[6]A. Ugur, F. Hatami, W. T. Masselink, A. N. Vamivakas, L. Lombez, and M. Atatüre, Appl. Phys. Lett. **93**, 143111 (2008).
[7]I. Luxmoore, E. D. Ahmadi, N. A. Wasley, A. M. Fox, A. Tartakovskii, A. B. Krysa, and M. S. Skolnick, Appl. Phys. Lett. **97**, 181104 (2010).
[8]D. Richter, R. Roßbach, W. Schulz, E. Koroknay, C. Kessler, M. Jetter, and P. Michler, Appl. Phys. Lett. **97**, 063107 (2010).
[9]M. Reischle, C. Kessler, W.-M. Schulz, M. Eichfelder, R. Roßbach, M. Jetter, and P. Michler, Appl. Phys. Lett. **97**, 143513 (2010).
[10]F. Hatami, W. T. Masselink, L. Schrottke, J. W. Tomm, V. Talalaev, C. Kristukat, and A. R. Goñi, Phys. Rev. B **67**, 085306 (2003).

[11]F. Hatami, W. T. Masselink, and L. Shrottke, Appl. Phys. Lett. **78**, 2163 (2001).
[12]W.-M. Schulz, M. Eichfelder, R. Roßbach, M. Jetter, and P. Michler, J. Cryst. Growth **315**, 123 (2011).
[13]W.-M. Schulz, R. Roßbach, M. Reischle, G. J. Beirne, M. Bommer, M. Jetter, and P. Michler, Phys. Rev. B **79**, 035329 (2009).
[14]S. Gerhard, V. Baumann, S. Höfling, and A. Forchel, Nanotechnology **20**, 434016 (2009).
[15]R. Leon, C. Lobo, T. Chin, J. Woodall, S. Fafard, S. Ruvimov, Z. Liliental-Weber, and M. A. S. Kalceff, Appl. Phys. Lett. **72**, 1356 (1998).
[16]S. Gerhard, S. Kremling, S. Höfling, L. Worschech, and A. Forchel, Nanotechnology **22**, 415604 (2011).
[17]Y. Song, P. J. Simmonds, and M. L. Lee, Appl. Phys. Lett. **97**, 223110 (2010).
[18]T. N. Tranh, C. Robert, C. Cornet, M. Perrin, J. M. Jancu, N. Bertru, J. Even, N. Chevalier, H. Folliot, O. Durand, and A. Le Corre, Appl. Phys. Lett. **97**, 223110 (2010).
[19]K. Rivoire, A. Faraon, and J. Vučković, Appl. Phys. Lett. **93**, 063103 (2008).
[20]Y. Akahane, T. Asano, B. Song, and S. Noda, Nature (London) **425**, 944 (2003).
[21]A. R. A. Chalcraft, S. Lam, D. O'Brien, T. F. Krauss, M. Sahin, D. Szymanski, D. Sanvitto, R. Oulton, M. S. Skolnick, A. M. Fox, D. M. Whittaker, H. Y. Liu, and M. Hopkinson, Appl. Phys. Lett. **90**, 241117 (2007).
[22]Y. P. Varshni, Physica (Amsterdam) **34**, 149 (1967).
[23]D. Englund, D. Fattal, E. Waks, G. Solomon, B. Zhang, T. Nakaoka, Y. Arakawa, Y. Yamamoto, and J. Vučković, Phys. Phys. Lett. **95**, 013904 (2005).
[24]K. Rivoire, Z. Lin, F. Hatami, W. T. Masselink, and J. Vučković, Opt. Express **17**, 22609 (2009).
[25]K. Rivoire, S. Buckley, F. Hatami, and J. Vučković, Appl. Phys. Lett. **98**, 263113 (2011).
[26]K. Rivoire, Z. Lin, F. Hatami, and J. Vučković, Appl. Phys. Lett. **97**, 043103 (2010).
[27]M. W. McCutcheon, D. E. Chang, Y. Zhang, M. D. Lukin, and M. Loncar, Opt. Express **17**, 22689 (2009).